Altered sense of self during seizures in the posteromedial cortex

Josef Parvizi[a,b,1], Rodrigo M. Braga[a,b], Aaron Kucyi[a,b], Mike J. Veit[a,b], Pedro Pinheiro-Chagas[a,b], Claire Perry[a,b], Clara Sava-Segal[a,b], Michael Zeineh[c], Eric Klaas van Staalduinen[c], Jaimie M. Henderson[d], and Matthew Markert[a,b]

[a]Stanford Human Intracranial Cognitive Electrophysiology Program, Stanford University, Stanford, CA 94305; [b]Department of Neurology and Neurological Science, Stanford University, Stanford, CA 94305; [c]Department of Radiology, Stanford University, Stanford, CA 94305; and [d]Department of Neurosurgery, Stanford University, Stanford, CA 94305

Edited by Marcus E. Raichle, Washington University in St. Louis, St. Louis, MO, and approved April 26, 2021 (received for review January 11, 2021)

The posteromedial cortex (PMC) is known to be a core node of the default mode network. Given its anatomical location and blood supply pattern, the effects of targeted disruption of this part of the brain are largely unknown. Here, we report a rare case of a patient (S19_137) with confirmed seizures originating within the PMC. Intracranial recordings confirmed the onset of seizures in the right dorsal posterior cingulate cortex, adjacent to the marginal sulcus, likely corresponding to Brodmann area 31. Upon the onset of seizures, the patient reported a reproducible sense of self-dissociation—a condition he described as a distorted awareness of the position of his body in space and feeling as if he had temporarily become an outside observer to his own thoughts, his "me" having become a separate entity that was listening to different parts of his brain speak to each other. Importantly, 50-Hz electrical stimulation of the seizure zone and a homotopical region within the contralateral PMC induced a subjectively similar state, reproducibly. We supplement our clinical findings with the definition of the patient's network anatomy at sites of interest using cortico-cortical–evoked potentials, experimental and resting-state electrophysiological connectivity, and individual-level functional imaging. This rare case of patient S19_137 highlights the potential causal importance of the PMC for integrating self-referential information and provides clues for future mechanistic studies of self-dissociation in neuropsychiatric populations.

self-dissociation | epilepsy | default mode network | posterior cingulate | Brodmann area 31

The posteromedial cortex (PMC) includes Brodmann areas (BAs) 23 (posterior cingulate), BA 29/30 (retrosplenial cortex), and BA 31 (Fig. 1*A*). The PMC is a core hub of a distributed brain network known as the default mode network (DMN; Fig. 1*B*) (1–4). The PMC shows increased activity during tasks involving self-referential processing, such as episodic memory retrieval (5), and its activity also increases during spontaneous thought (6), which often involves recollections about personal experiences as well as self-related thoughts regarding the future (7, 8). This lies at the core of "internal chatter" in our brain for reflecting on our decisions, reappraising our emotions, simulating alternative futures, reminiscing about the past, and continually updating the personal narrative about sense of our self (9). By contrast, many conditions which share a requirement for externally directed attention lead to reduced activity within the PMC (10). Furthermore, metabolic studies indicate that the PMC is among the most active sites of the brain during a resting state, consuming about 35% more glucose than other brain regions (11). The PMC shows profound deactivation during propofol-induced anesthesia (12) and is the first region of the brain to increase its activity in patients regaining consciousness from an unconscious state (13).

A comprehensive anatomical tracing study in nonhuman primates (14) revealed a strong connection between PMC and anterior cingulate cortex, posterior parietal cortex, prefrontal cortex, basal forebrain, claustrum, basal ganglia, brainstem, and the thalamus. This study also confirmed that different subregions of the PMC have distinct patterns of interconnectivity among each other (Fig. 1*C*) and with the rest of the brain. For instance, retrosplenial cortex has preferential connections with limbic structures, such as the amygdala, hippocampal formation, orbitofrontal cortex, periaqueductal gray matter, and nucleus accumbens. Most relevant to our current report, BA 31 receives dense projections from the medial parietal area 7m (which has strong connections with sensory motor structures) and also from BA 23 and by the virtue of such strong incoming connections may serve anatomically as a site of convergence of projections from the cingulate and parietal cortices.

Importantly, the connectivity pattern of the PMC with the thalamus is very unique in that the PMC projections target the entire dorsal mantle of the thalamus from the very posterior to the most anterior-associative nuclei of the dorsal thalamus (14) (Fig. 1*D*). In the most anterior part of the thalamus, the PMC projections reach the anterior thalamic nuclei bilaterally. These nuclei of the thalamus are key recipients of massive bilateral projections from the subicular cortices (15) thought to be relaying memory-related information. In summary, the PMC has the means by which to influence all thalamocortical loops operating ipsilaterally from the dorsal-associative thalamic nodes and bilaterally from the anterior, thalamic regions. The thalamus is known to be one of the subcortical nodes of the DMN (16).

Despite a wealth of neuroimaging data from the PMC, we have little causal information regarding the function of the PMC. This is in part because lesions following a stroke do not often affect the PMC, given its redundant arterial supply (Fig. 1*E*). Branches

Significance

In this manuscript, we report a rare case of a patient with localized seizures originating from the right anterior and dorsal posteromedial cortex (PMC). We mapped the electrophysiological and neuroimaging connectivity of the ictal onset site and replicated seizure auras by stimulating the homotopical PMC site in the left hemisphere. Our findings provide a causal link between PMC and the sense of self and provide unique clues about the pathophysiology of self-dissociation in neuropsychiatric conditions.

Author contributions: J.P. designed research; J.P., R.M.B., A.K., M.J.V., P.P.-C., C.P., C.S.-S., M.Z., E.K.v.S., J.M.H., and M.M. performed research; R.M.B., M.Z., E.K.v.S., J.M.H., and M.M. contributed new reagents/analytic tools; J.M.H. performed neurosurgical operation; J.P., R.M.B., A.K., M.J.V., P.P.-C., M.Z., E.K.v.S., J.M.H., and M.M. analyzed data; and J.P. and M.M. wrote the paper.

The authors declare no competing interest.

This article is a PNAS Direct Submission.

[1]To whom correspondence may be addressed. Email: jparvizi@stanford.edu.

This article contains supporting information online at https://www.pnas.org/lookup/suppl/doi:10.1073/pnas.2100522118/-/DCSupplemental.

Published July 16, 2021.

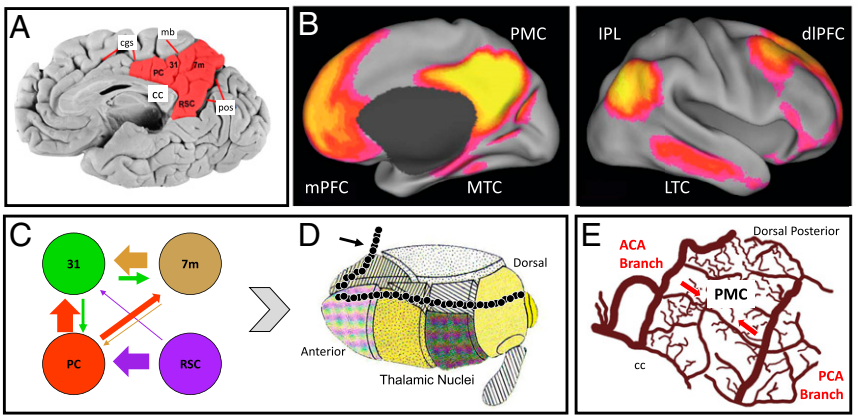

Fig. 1. Functional and anatomical connections and blood supply of PMC. (*A*) Resting-state fMRI reveals a strong connectivity between PMC and a set of regions that are commonly referred to as the DMN. (*B*) The PMC includes cytoarchitecturally distinct subregions referred to here as the posterior cingulate (PC; Broadman area BA 23) and the retrosplenial cortex (RSC; BA 29/30), as well as the medial parietal cortex (BA 7) and the BA 31. (*C*) PMC subregions are anatomically interconnected, with BA 31 being a major recipient of projections from other subregions of the PMC. (*D*) The PMC projects to the anterior–posterior mantle of the dorsal-associative nuclei of the thalamus ipsilaterally (black dots) and the anterior nuclei of the thalamus bilaterally (black arrow) and thus influencing the activity of multiple thalamocortical loops. (*E*) The PMC is protected from ischemic stroke lesions because of blood supplies from both anterior and posterior circulations. Abbreviations: ACA = anterior cerebral artery; CC = corpus callosum; cgs = cingulate sulcus; IPL = inferior parietal lobule; LTC = lateral temporal cortex; mb = marginal branch of cingulate sulcus; mPFC = medial prefrontal cortex; MTC = medial temporal cortex; PCA = posterior cerebral artery; and pos = parietooccpital medial sulcus. *A* is modified from Yeo et al. (46); *B–D* are modified from ref. 14; and *E* is a drawing based on ref. 17. dlPFC, dorsolateral prefrontal cortex.

from the anterior circulation (pericallosal/precuneal branches of anterior cerebral artery) and the posterior circulation (parietooccipital branch of posterior cerebral artery) supply the PMC and anastomose together, and these branches even cross the hemisphere and supply the contralateral PMC in about 20% of cases (17, 18).

The anatomical location of the PMC (i.e., buried in the interhemispheric fissure and encased by the sagittal sinus and bridging veins) makes this territory especially difficult to target using transcranial stimulation methods. In contrast, direct application of intracranial electrical stimulation (iES) provides a viable alternative in which a volley of electrical discharges can be delivered directly to a given PMC subregion in awake human subjects. This stimulation can be probed with a subjective report or task performance. This method provides a reliable measure of causality that has garnered considerable attention since the works of pioneers such as Otfrid Foerster, Charles Sherrington, and notably their student Wilder Penfield (19, 20).

PMC is notorious for its frequent unresponsiveness to electrical stimulation. The number of attempts by us (21) and others (22) stimulating PMC have largely resulted in null results in terms of changes in subjective experience. We recently explained these null results in terms of the DMN's placement at the top of the large-scale cortical gradient, extending from sensory-oriented to associative networks (23). A recent study claimed impairment in episodic encoding when the posterior cingulate/retrosplenial cortex region was electrically stimulated (24). However, as noted in a commentary (25), the study did not examine the effect of stimulation on a control task, or in a control region of the brain, and as such it remains possible that the observed effects were neither specific to the PMC nor to episodic encoding.

Another means for obtaining causal information is to study patients with seizures involving a given brain region and study the subjective reports given by those patients. Epileptologists often rely on such experiential reports to locate the seizure onset and symptomatogenic zones within individual patients, with accuracy determined in retrospect by postsurgical seizure freedom after excision. For instance, patients with the tingling of a given limb during seizures often have electrographic activity either originating from or propagating through the somatosensory network. Likewise, patients with visual auras are thought to have occipital seizures affecting the visual network, and those with emotional auras are thought to have seizures involving limbic regions. Interestingly, seizure behavior or subjective reports respect a high degree of stereotypy in a given patient or across patients with similar epilepsies (26).

Reports of PMC seizures have been rare in the literature (27–36). Bancaud and Talairach (27) were the first to describe a typical syndrome characterized by a "incomplete loss of consciousness" attributed to possible posterior cingulate epilepsy. Other reported cases of PMC seizures have been characterized by "staring and unresponsiveness" (29), "consciousness impairment" (31), and "body image disturbance and spatial displacement" (34, 37). Alkawadri and colleagues (30) studied a larger series of patients with cingulate gyrus seizures and reported two cases of posterior cingulate seizures with the subjective feeling of falling in one case and "depersonalization" in another. Unfortunately, in some of the reported cases, the terms "precuneus" and "posterior cingulate" were used interchangeably, while some others used the broader lens of "parietal cortex epilepsy." In all the reported cases, however, detailed reports of patients' subjective experience during seizures were not made available.

A recent rare case of a patient gave us the unique opportunity to fill an existing gap of knowledge and explore a causal link between the PMC, a core region of the DMN, and the subjective "sense of self." While this case was briefly mentioned as part of a recent publication on optogenetic work in mice, confirming a link between rodent PMC oscillatory dysfunction and the phenotype of self-dissociation–like behavior (38), the current report provides additional details, which we hope will add unique causal information to the extant literature.

Results

Subject. We evaluated a young patient in his 20s (Patient S19_137) who was a high-functioning executive in a Silicon Valley startup. His epilepsy first presented itself at the age of 10 but was relatively well controlled with medications until he experienced increased seizure frequency, medication side effects with escalating dosages, and a significant reduced quality of life in the years prior to his referral to the Stanford Comprehensive Epilepsy Program in 2019.

Scalp Electroencephalography Findings. Around 1 y prior to intracranial monitoring, the patient's seizures were captured during

video scalp electroencephalography (EEG) monitoring at another institution. Four focal nocturnal seizures and one focal-to-bilateral seizure were captured presumably with right posterior and central onset. About 7 y earlier, similar monitoring had captured five typical seizures with retained awareness of possibly right central parietal seizure onset location. His seizures were considered incompletely localized on scalp electrodes. During his first day of video EEG monitoring in 2019, 40 focal aware seizures were captured with midline (Cz and Pz) onset, followed by right hemispheric, rhythmic activity. Using high-density EEG recordings with 256 electrodes, we captured four awake and two nocturnal seizures but could not clearly localize the source. Analysis of single spikes ($n = 10$) revealed possible left medial frontal central (Fz) spikes.

Clinical Imaging Findings. Intracranial EEG (iEEG) monitoring with depth electrode placement was conducted. Electrodes were placed in the PMC, medial frontal cortex (MFC), lateral posterior parietal cortex, mesial and lateral temporal lobes, and anterior and left posterior insula (Fig. 2*A*). The left MFC was robustly sampled because of the high-density EEG findings noted earlier. As part of a comprehensive diagnostic evaluation, high-resolution three-Tesla (3T) MRI was interpreted as nonlesional (Fig. 2*B*). Functional MRI (fMRI) revealed a strongly left-lateralized language function (Fig. 2*C*). Ictal single-photon emission computed tomography showed increased perfusion in posterior midline structures, basal ganglia, and anterior temporal lobe, but this study was deemed less reliable, given that the patient was having seizures almost every hour.

Clinical Intracranial EEG Findings. Intracranial EEG recordings revealed an unequivocal focal source of epileptic spikes and seizures in the right PMC, adjacent to the marginal branch of the cingulate sulcus, most likely corresponding to BA 31 (electrode RC in Fig. 2). Of note, the left PMC was not the source of spontaneous clinical seizures. Sample recordings are shown in *SI Appendix*, Fig. S1. In total, 17 seizures were captured during sleep and wakefulness, and all originated from the PMC (i.e., recording sites RC4, RC5, and RC6) and propagated to the homotopical region on the left hemisphere (electrode LJ), as well as MFC and temporal regions. The patient's seizures were classified as focal aware seizures with cognitive onset that generalized to tonic events. The patient received responsive neurostimulation (RNS) therapy (NeuroPace). Two RNS electrodes targeted the RC3 to RC6 site and the neighboring cortical region. Prior to surgery, the patient was having minimum two seizures per day but after RNS therapy his seizures have been reduced by at least 70% and occur almost always at night. The RNS device has reliably captured seizures in the RC site (*SI Appendix*, Fig. S1).

Patient Subjective Report of Seizures. Prior to onset, the patient would sense that a seizure was going to start. He denied any physical symptoms or auras typically associated with limbic seizures. He had intact insight and remained alert throughout his seizures, but according to his own description of the events, he was left as "an observer of an active, internalized experience over which I have little control." He had memory retention for the information presented during seizures and would give long and very specific descriptions of his inner cognitive experience. In the patient's own words, during seizures "the system I know as 'myself' leaves my body." He reported "self-dissociation" by stating that "I listen to two parts of my brain speak to each other in a way that a third part of my brain, which I consider to be 'me,' is able to listen. . .I had to go through the steps of refiguring it out by listening to another conversation in my brain. Like two independent computer components talking to each other, but the CPU. . .[i.e.,] 'me' was just the observer. The other parts of my brain that were talking—I stopped considering them 'me'—it was exactly like if you were listening to a different person inside your head."

Along with these cognitive symptoms, the patient almost always experienced a loss of spatial awareness (i.e., his position in space), which was a key component affecting his gait stability. He detailed at length how the onset of his seizure was a physical awareness of a change in his spatial relationship to the six cardinal directions (x-, y-, and z-axes) ". . .I could feel them move in rotation. . .like you feel when you're falling but in all directions." If he was standing, he would remain alert and typically would continue to speak but would feel that he had become imbalanced and would express a sense of fear or dread for not knowing his position in space. During this experience, he would become focused on coming in contact with a wall or furniture. The patient reported sometimes adopting a strategy of dropping objects in view to observe how they fell or bounced, which helped him regain his sense of space, and determine visually what is up and what is down. Patient reported this would help him "reorient" and viewed it as an expression of control in reassociating with reality: "If I demonstrate to the other parts of my brain what is real, I can convince [the people talking in my head]—so when I can see a pen drop, it's like I know which way is down now." On completion of some such tasks, he would appear to have a rapid reorientation and a reduction in physical expression of discomfort or imbalance. His seizure would subside, and he could continue his conversation as normal. These dissociative events with retained awareness would typically last less than 30 s, with some variability affected by his behavior. Other seizures could rarely progress to tonic events. With medication withdrawal during hospital testing, he experienced a loss of awareness and generalized bilateral stiffening (tonic) and jerking (clonic) activity and postictal confusional period (Movie S1)

Intracranial Electrical Stimulation. As part of a routine clinical mapping procedure aimed at determining regional function and potential involvement in seizure onset, select electrode contacts were stimulated using iES (39). Details of this procedure are provided in *SI Appendix*, Table S1. The patient's response is reported ad verbum. The reproducible feelings of "auras" were solicited with reliability when electrodes RC1 to RC5 within the PMC—but not other electrodes—were stimulated. Importantly, stimulation of the medial or lateral temporal lobes, insula, or MFC did not reproduce any signs of auras. Upon stimulation of the left PMC (electrode LJ5; Fig. 2), the patient reported reoccurrence of those feelings experienced during his seizures saying, "That was the same dissociation [as my seizures]. . .closest to my episodes you initiated." When the left PMC stimulation was repeated, he reported again, "That's exactly like I was describing [about my seizures]." Elaborating on the experience further, he explained, "What you created [with the stimulation] was that separation, but not of my control over my body. . .the same way a pilot can lose control of a plane. They can be forced out of the cockpit. . . or forced to not control it but still see what's happening to the whole plane. That's what just happened. I got pulled out of the cockpit. . .or I got pulled out of the chair, the pilot's chair, but I could still see all the gauges. . .what you did was move me out of that chair a little bit." When asked by the neurologist physician (J.P.) "Were you floating in space?", the patient replied, "No. I was floating more in myself." When asked to compare the stimulation effects to his seizure, the patient noted that the stimulations were "close" and "a nice version of the seizure, cleaner. . .I would describe it as a portion of the curve of my episode." He said there was some difference, because during the stimulation "if I wanted to take control, I could have," which is not the case during the climax of one of his seizures. We attribute this to the careful management of current delivery possible with direct cortical stimulation.

Experimental Cognitive Intracranial EEG Findings. The patient participated in experimental tasks of episodic memory recall, in which the subject was presented with simple mathematical equations

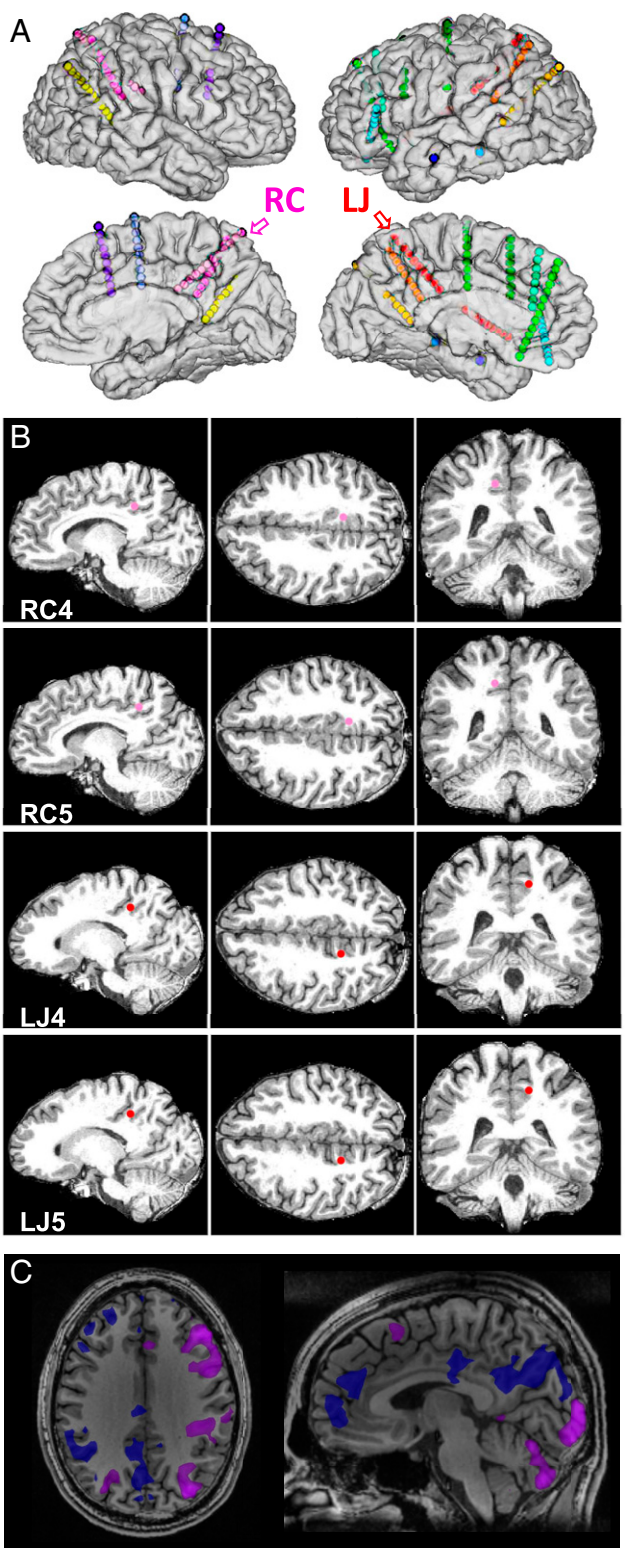

Fig. 2. Localization of the implanted electrodes and language areas. (*A*) Three-dimensional reconstruction of the patient's preoperative MRIs, with colocalization of the implanted electrodes. Different colors have no specific connotations. Note the location of the RC and LJ electrode shafts on the right and left hemispheres, respectively, that traverse from the anterior ventral to dorsal posterior extent of the PMC. The edge-to-edge distance between electrodes contacts is only 2.71 mm. (*B*) The high-resolution 3T structural images in sagittal, axial, and coronal views with the position of the electrodes of interest. (*C*) Clinical, functional imaging procedure depicted in the axial and sagittal planes show the activation maps during object naming denoting the left hemisphere as the patient's language-dominant hemisphere (uncorrected voxel-wise T score of 4 [$P = 0.00006$]), with a minimum cluster threshold of 3 pixels). Note the right PMC and MFC deactivations during this language task.

(e.g., 2 + 6 = 9) or self-referential, autobiographical statements (e.g., "Today, I drank coffee") and was asked to judge the accuracy of these statements with a button press (1 for correct or 2 for incorrect) and when a crosshair was present on a black screen (5, 10, and 15 s) do nothing. As shown in *SI Appendix*, Fig. S2, responses to episodic recall were seen in some of the PMC contacts but not in the seizure onset or the relevant PMC iES sites.

Connectivity and Network Mapping. The observation that stimulation of the contralateral PMC could recapitulate the unusual and specific seizure symptoms raised the possibility that these sites of interest in RC and LJ shafts of electrodes must be 1) strongly interconnected and 2) part of the same network. To address these hypotheses, we investigated the functional organization near to the seizure onset site on the right PMC as well as the homotopical contralateral nonepileptic site, whose electrical stimulation caused a sense of self-dissociation. For this, we used three different methods: electrophysiological resting-state connectivity, cortico-cortical–evoked potentials (CCEPs), and fMRI resting-state connectivity.

First, in line with previous iEEG work (40–43), we tested the connectivity between the two sites of interest electrophysiologically by correlating the slow (0.1 to 1.0 Hz) fluctuations of high-frequency (>70 Hz) resting-state and task-induced iEEG signal between all electrode contacts on RC and LJ sites. Although both RC and LJ electrode shafts shared a similar trajectory in each hemisphere, contacts situated within the PMC (RC1 to RC5 and LJ1 to LJ4) showed higher pair-wise correlations (Fig. 3*A* and *SI Appendix*, Fig. S3). This supports that the sites of interest were within brain regions that were strongly interconnected.

Next, we measured CCEPs (44, 45) in which 40 single-pulse stimulations (below the threshold of subjective awareness) were delivered with 8-mA current and 0.5-Hz frequency in the seizure onset zone (RC4 to RC 5), while recording the timing of evoked responses (if present) in other electrode sites. Of all the contacts, the ipsilateral PMC electrodes (RC and RD) and contralateral PMC sites (LJ) showed the lowest latency time to peak (Fig. 3*B*). When RC4 to RC5 was stimulated, the average time to peak of evoked potentials across the contralateral LJ sites was 44.9 ms with an SE of 13.3 ms, suggesting the presence of strong and direct anatomical connections between the two PMC sites of interest.

While the first two methods established electrophysiological connectivity between the two PMC sites of interest, we used functional imaging data to test the hypothesis that the RC and LJ sites were part of the same large-scale connected network. We first superimposed the two PMC sites on a commonly referenced map of the DMN, defined using data collected from 1,000 individuals (46). Relative to this group-averaged map, both the seizure and contralateral PMC sites were located within the boundaries of the DMN, near to the dorsal border of the PMC region (Fig. 3*C*). Next, we estimated the anatomy of the DMN using methods optimized for network definition within individuals (47–49).

Network definition and identification was performed by a trained expert (R.M.B.). Our previous analyses of individual-level anatomy have revealed that within canonical DMN regions, two distinct networks, referred to as "DN-A" and "DN-B," can be resolved (see detailed descriptions of the anatomy of each network in refs. 47 and 48). This finding has now been confirmed in multiple individuals (50, 51). Here, the aim was to recapitulate these previous observations in patient S19_137 to best estimate their idiosyncratic network organization within PMC. Network definition was

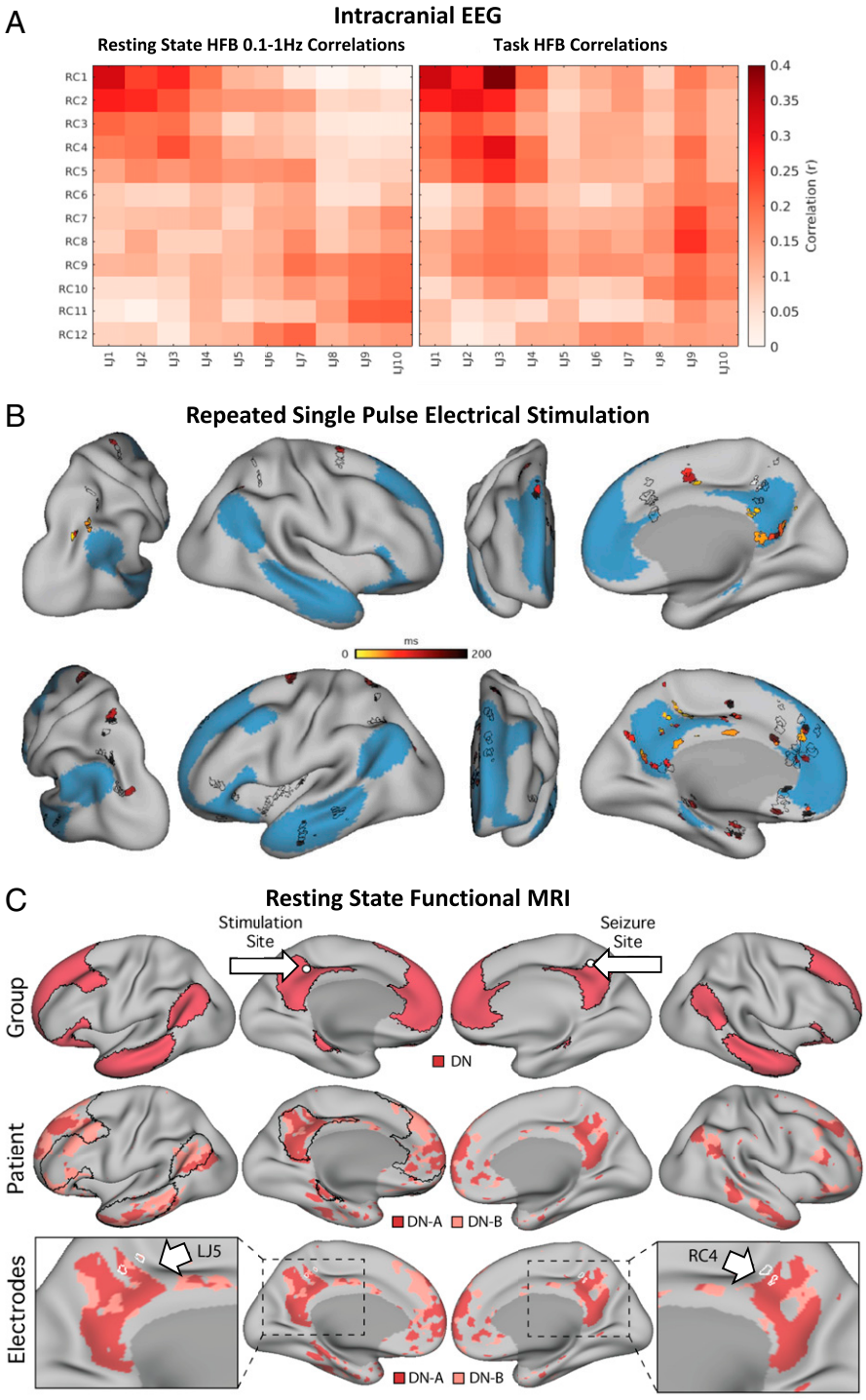

Fig. 3. Connectivity and network mapping. (*A*) Electrophysiological connectivity during rest (*Left*) and experimental task (*Right*). iEEG functional connectivity matrices are shown for the interelectrode correlations of slow (0.1 to 1 Hz) fluctuations of high-frequency (70 to 170 Hz) power amplitude for RC versus LJ electrodes that traverse through the PMC. Resting-state (*Left*) and task (*Right*) correlations are based, respectively, on mean correlations across four runs of resting state (20.3 min total) and three recording runs during an experimental task of attention (15.3 min total). (*B*) Electrophysiological connectivity during repeated single-pulse electrical stimulation. The time to peak of evoked potentials from single-pulse stimulation of the seizure origin site are shown here. For this analysis, we delivered repeated single pulses between RC4 and RC5 and recorded from all other electrodes (areas bounded by black lines). Electrodes, which did not show any significant evoked responses, are shown as black borders with no filled color. In electrodes in which a significant response was noted, the color corresponds to the time to peak of the evoked response. Note how stimulation in RC4 to RC5 evokes rapid responses in homotopical PMC electrodes. (*C*) fMRI resting-state connectivity. Network organization was estimated first using a group-averaging approach [*Top* row; data from Yeo et al. (46)], then methods were optimized for network definition within individuals (*Middle* row). When networks are defined within individuals, two parallel networks (DN-A and DN-B) can be defined within default network regions, both of which typically contain regions falling within the bounds of the canonical default network. In patient S19_137, the two networks were successfully defined, both of which fell within the group-defined default network (black lines in *Middle* row) and recapitulated known features of the networks (detailed in *Materials and Methods*). Both the seizure origin and contralateral stimulation sites of interest (white borders on *Lower* row) overlapped with functional regions related to the default network as defined by both methods.

performed using two approaches: manual seed-based functional connectivity and data-driven clustering. Both approaches produced a similar distribution of network regions for both DN-A and DN-B (*SI Appendix*, Fig. S4). Seed regions were manually chosen using an iterative process. Initially a seed was placed in the posterior parahippocampal cortex to estimate the anatomy of network DN-A. When a seed was found which showed robust correlations with a distributed network that included regions in retrosplenial and posterior cingulate cortices, as well as dorsolateral prefrontal cortex, angular gyrus, and lateral temporal cortex, this seed location (i.e., vertex number) was recorded.

The topography of correlated regions from this medial temporal seed was then used to inform the selection of subsequent seeds from the dorsolateral prefrontal cortex. A pool of candidate seeds was recorded from the dorsolateral prefrontal cortex, each recapitulating the observed features from the medial temporal seed, as well as previously characterized features of DN-A. The correlation maps from these candidate seeds were compared visually, and a single frontal seed was selected that was deemed to best capture the anatomy of DN-A, with robust correlations in the characteristic regions and low correlations elsewhere. This seed became the representative estimate of DN-A in patient S19_137 (shown in *SI Appendix*, Fig. S4). A similar iterative process was used to identify DN-B from dorsolateral prefrontal seeds, though for this network the anatomy of DN-A served as a guide for navigating this patient's functional anatomy (47, 48). In each case, the experimenter's prior knowledge of the anatomy of each network in previously tested individuals was used to guide seed selection. Data-driven parcellation (k-means clustering at $k = 16$) was used to confirm the topography of the networks in a manner that reduces potential experimenter bias by removing the need for manual selection of seeds. The k-means clustering was performed using multiple values of k, starting at $k = 12$ through $k = 20$. Clustering solutions were checked in ascending order by R.M.B., and the lowest k solution, which recapitulated the separation between DN-A and DN-B (as observed in the seed-based maps), as well as an adjacent language network (not studied here), was taken ($k = 16$; Fig. 3).

In line with earlier observations (47, 48), within patient S19_137, we were able to identify two distinct networks within the DMN (DN-A and DN-B). Regions belonging to both networks fell largely within the group-defined DMN boundaries (Fig. 3), and both networks displayed interdigitated regions in multiple zones of the cortex. DN-A included a ventral PMC region that extended into the retrosplenial cortex and contained a region in parahippocampal cortex, while DN-B contained a region in the posterior cingulate cortex that was surrounded by regions belonging to DN-A. In the parietal lobe, DN-A contained a region in posterior angular gyrus, positioned next to a more anterior DN-B region, as expected from previous findings. These observations helped build confidence that the within-subject definition of distributed networks in this patient was successful.

The location of the two electrode sites of interest were next overlaid onto the maps of DN-A and DN-B (Fig. 3). Each electrode's sampling volume was approximated by generating a 4-mm diameter sphere at the manually identified centroid of each electrode contact location. Each sphere was projected to the cortical surface using FreeSurfer (52) for easier visualization of how the estimated network boundaries related to the sampling volumes on the cortical sheet. The analyses revealed that both sites overlapped in part with DN-A, as defined in this individual (Fig. 3). The left site (LJ4) was also situated near to a small region of DN-B, which was also observed in the seed-based map (*SI Appendix*, Fig. S4). Interestingly, both sites also overlapped with regions just outside of the DMN, likely within the marginal branch of the cingulate sulcus. Hence, stimulation of each of these sites may have also affected neighboring systems.

Together, these data from three independent modalities confirm that the seizure onset region on the right and the positive stimulation sites on the left were physiologically connected and possibly were also part of the same large-scale distributed network (i.e., DMN). Our findings also reveal a plausible functional pathway through which seizure activity (and electrical discharges induced by iES) could elicit dissociation experiences in this patient.

Discussion

Here, we report the case of a unique individual patient with seizures originating in the PMC, a brain region canonically associated with DMN, whose seizure semiology was characterized by an altered sense of self. This condition resembled a state of self-dissociation in which the patient had an experience of "depersonalization (i.e., unreality, detachment, or being an outside observer with respect to one's thoughts, feelings, sensations, or body)," "while reality testing remained intact"—as self-dissociation is defined in the *Diagnostic and Statistical Manual of Mental Disorders Fifth Edition* (53). During seizures, he repeatedly tried to do things (such as throwing a blanket on himself to make sure that he can feel his body) to regain a sense of reality.

Using intracranial recordings and experimental data, we mapped the presumed network of cortical regions that the patient's seizures might have engaged. We found evidence for short-latency connections between the source (i.e., the right PMC) and the homotopical contralateral nonepileptic site. We also found evidence that the epileptic network may be embedded within a broader functional organization that comprises distributed networks that are located within canonical DMN regions.

We believe that the state of self-dissociation was caused by the recruitment of bilateral PMC and a distributed network of brain regions that are anatomically or functionally connected with the PMC either directly or indirectly via the thalamus. In this regard, the role of cortico–thalamic connection of the PMC cannot be overemphasized (Fig. 1*D*). Of note, in a recent optogenetic study (38), it was shown that self-dissociative–like behavior in rodents, caused by ketamine infusion, led to pathological oscillatory activity not only in the posterior cingulate cortex but also in the dorsal thalamus and that the inhibition of the dorsal thalamic nuclei caused the exaggeration of the pathologic cortical, rhythmic activity.

Although our report is unique in showing self-dissociation during seizure auras and after stimulation of the PMC, there are key previous studies that are noteworthy in this regard. For instance, out of body experience (which is a form of self-dissociation) has been reported during stimulation of the right temporoparietal junction (TPJ) area (54, 55), which could be possibly related to perturbations in the interaction between the TPJ and PMC—a proposition that requires future investigations.

The findings from our individual patient can be best understood in the context of recent iEEG findings from the PMC. Intracranial recordings (with precise anatomical information at the level of single subjects) have suggested that the PMC in each individual brain is a heterogeneous collection of functionally distinct subpopulations of neurons, each of which has specific functional responses during experimental tasks. Such heterogeneous, functional organization within the PMC is evident at the millimeter scale, meaning that neuronal populations that are only 2 to 5 mm apart from each other may belong to distinct functional circuits (*SI Appendix*, Fig. S2). As we have summarized elsewhere (56) and detailed in a separate report (57), such information cannot be appreciated from imaging findings that rely on group-based volume averaging. For instance, we have shown that distinct PMC subpopulations of neurons in a given individual brain are activated during internally directed self-referential, episodic memory processing or during the transition to a cued-rest condition (i.e., a blank screen in which the subject is instructed to just relax and do nothing). The onset of activity during a memory condition is late and

close to the subject's response (300 to 500 ms), coinciding with the presentation of the recalled item (57). These populations also show jittered, slow, and gradual activations during spontaneous rest (5 min of mind wandering). By contrast, the onset of activation during the cued-rest condition is relatively fast (~100 to 200 ms)—too fast to be caused by mind wandering but perhaps crucial for its initiation. Such activations occur in transition from nonrest to cued rest and not vice versa (57, 58). Seldom do we see a memory-activated electrode site to also activate during cued rest (*SI Appendix*, Fig. S2). Interestingly, only some neuronal populations become deactivated during conditions of externally directed attention (57), and the extent of transient high-frequency broadband (HFB) suppressions is correlated with task complexity and subject performance (59). Lastly, and perhaps most relevant to our discussion, we have noticed repeatedly that in each single subject, some PMC sites are conspicuously silent during the conditions of self-referential recall or transition to cued rest, and during conditions of externally directed attention, they may not deactivate either. Such lack of response is present without any observed pathological epileptic activity in the PMC.

As noted in *SI Appendix*, Fig. S2, seizure onset electrodes (RC4 to RC6) or the relevant iES sites (LJ4 to LJ5) did not show any responses during self-referential memory recall. Such a lack of responses could be due to frequent epileptic activity in the seizure onset zone since we have previously shown that the function of an epileptic site is "seized" for ~800 ms before to 300 ms after pathological epileptic activity (60). However, this does not explain the lack of functional responses to self-referential processing at the site of electrical stimulation since that site was entirely void of any spontaneous epileptic activity. It is possible that the precise neuronal populations of interest in our current report are not activated directly during episodic memory condition, but perhaps, these neuronal populations might be involved in converging self-referential memory information from BA 23 and BA 29/30, with a spatial map of self from BA 7m (e.g., proprioceptive, vestibular, and visual information)—the combination of which may provide a foundation necessary for the construction or perception of a sense of self. The position of area 31 at the anterior and dorsal edge of PMC, close to sensorimotor and parietal areas, and its pattern of connectivity with other PMC subregions lend anatomical support for this hypothesis. We are mindful that this hypothesis needs future well-controlled experimental paradigms to be tested and hope that our unique patient's case will provide intriguing clues for such future explorations of the anatomy and physiology of sense of self.

Materials and Methods

Informed Consent and Institutional Review Board. The Stanford institutional review board committee has approved the experiments described in this report. Informed consent for experiments was obtained prior to surgery and by the research team.

Clinical EEG Recording and Electrical Stimulation. We used Nihon Kohden video EEG monitoring equipment (version WEE-1200 with 1,000-Hz sampling rate), Nihon Kohden Cortical Stimulator (MS-120BK-EEG), and PE-210AK Stimulator Switchbox to deliver electrical pulses at various frequencies, amplitudes, and pulse widths.

Electrodes. The patient was implanted with AdTech depth electrodes that were 0.86 mm in diameter with 2.29-mm contacts spaced 3 to 5 mm apart. RC and LJ electrodes were 5 mm apart. With spacing 5 mm center to center, the edge-to-edge distance between contacts is 2.71 mm.

Electrode Localization. Electrode contact locations were approximated by manually selecting contact centroids on the patient's computed tomography (CT) image using BioImage Suite. Electrode localization was performed by three independent raters (R.M.B., C.S.C, and S.K.), with an average interrater error of 0.31 mm (*SI Appendix*, Fig. S4). Registration of the CT image (containing information about the electrode locations and skull anatomy) to the anatomical T1 MR image (containing information regarding brain tissue anatomy) was performed using linear registration and implemented as part of the intracranial electrode visualization suite. Registered images were carefully visually checked to ensure that adequate registration had been achieved. See examples of slices shown in *SI Appendix*, Fig. S5, in which the outline of the pial surface (obtained from the T1) can be seen to precisely fit within the bounds of the skull (as seen in the CT image), despite the complex anatomy of the cortical surface.

MRI Data Acquisition. Data were acquired at the Stanford University Richard M. Lucas Center for Imaging on a 3T General Electric SIGNA Premier scanner using a 48-channel head coil (GE Healthcare). Blood oxygenation level–dependent (BOLD) fMRI data were acquired using a simultaneous multislice gradient echo echo-planar pulse sequence. Sequence parameters were similar to those used as part of the Human Connectome Project: TR (Repetition Time) 1,000 ms, TE (Echo Time) 30 ms, flip angle 64°, 2.4 mm isotropic voxels, matrix 88 × 88 × 65, and multislice 5× acceleration. Minimization of signal dropout was achieved by visually selecting a slice plane ~25° from the anterior–posterior commissural plane toward the coronal plane. A T1-weighted anatomical scan was acquired in each session using a three-dimensional fast spoiled gradient echo sequence: TR 1,891 ms, TE 1.172 ms, TI 400 ms, flip angle 11°, 1.0 × 1.0 × 1.2 mm voxels, and matrix 256 × 192 × 132. A gradient echo B0 field map was acquired to correct for spatial distortions: TE 6.5 and 8.5 ms, with slice prescription/spatial resolution matched to the BOLD sequence.

Data collected during a visual fixation task were used for functional connectivity analysis. The patient fixated on a black "+" symbol presented at the center of a light gray screen. The patient was asked to remain as still as possible and to remain awake and focused throughout the duration of each run. In between runs, the patient was asked if he was able to successfully stay still during the previous run to reinforce the expectation that this should be closely monitored. Each run lasted 7 min 2 s, and three functional runs were collected. The raw data were visually checked for motion and scanner artifacts prior to data analysis. Maximum framewise displacement ranged from 0.543 to 0.586 mm, mean framewise displacement ranged from 0.122 to 0.142 mm, and voxel-wise temporal signal to noise ratio ranged from 20.8 to 22.3 mm. Given the stability of these data quality metrics across runs and the absence of any visual artifacts in the data, no runs were excluded. This yielded a total of 21 m 6 s of fMRI data for functional connectivity analysis.

For the clinical fMRI, data were collected also on a 3T GE 750 MR Discovery scanner. The patient performed an object naming task, which consisted of 12 blocks of 10 s of naming objects approximately every 3 s, alternating with rest blocks, during echo-planar imaging at 3 mm isotropic resolution.

MRI Data Preprocessing. BOLD data were preprocessed using procedures designed to optimize alignment of data acquired over multiple runs from the same individual and to minimize spatial blurring by avoiding multiple interpolation steps. The "iProc" pipeline was used, which is described extensively in ref. 47, and expands upon procedures developed in ref. 48. To aid data alignment, two patient-specific normalization templates were created: a mean BOLD template and a T1 anatomical template. The mean BOLD template was created by first selecting an example BOLD frame (the middle volume) from the first acquired run. This volume was upsampled to 1.2-mm isotropic resolution to improve registration. BOLD data from all three runs were then registered to this example volume, and an average was calculated across runs, meaning that data from all runs was used to create the mean BOLD template. This served to reduce bias toward any particular run. The T1 anatomical template was created by upsampling the acquired T1 image to 1.0-mm isotropic resolution.

For each BOLD volume, registration matrices were calculated to 1) correct for head motion, 2) correct for geometric distortions due to magnetic susceptibility effects using the acquired field map, and 3) register data to the mean BOLD template. A further linear registration matrix was calculated once to register the mean BOLD template to the T1 anatomical template. Next, for each BOLD volume, the four registration matrices were transposed into a single matrix and applied. This projected the BOLD data to the T1 anatomical template in a single interpolation step to reduce blurring. The resulting aligned BOLD data were thus upsampled to 1 mm isotropic space, which we have also previously found to help with observing detailed functional anatomic features.

Nuisance variables were regressed out of the data for functional connectivity analysis and included six motion parameters plus whole-brain, ventricular, and deep white matter signal, as well as their temporal derivatives. These signals were regressed out of native space–projected BOLD data (using 3dTproject; AFNI v2016.09.04.1341; Cox 1996; 2012), followed by

bandpass filtering at 0.01 to 0.1 Hz (using 3dBandpass; AFNI v2016.09.04.1341; Cox 1996; 2012). The white matter and pial surfaces were calculated from the T1 anatomical template using FreeSurfer's recon-all (52). Data were resampled from the native space to the fsaverage6-standardized cortical surface mesh (containing 40,962 vertices per hemisphere; using mri_vol2surf). Data were sampled from the gray matter at a position halfway between the white and pial surfaces using trilinear interpolation. Data were smoothed along the surface using a 3 mm Full Width at Half Maximum (FWHM) kernel. Data were initially smoothed at 2 mm FWHM; however, we found that the resulting functional connectivity maps displayed granular regions at lower correlation values and were less likely to show robust long-distance correlations. The decision to use 3 mm FWHM was made prior to the network identification analyses described.

Definition of Electrode Contact Regions of Interest. Electrode contact locations were established in relation to the anatomical information provided by the T1 anatomical template (see *Electrode Localization*). At each electrode centroid, a 2-mm radius sphere was generated using fslmaths to create an electrode contact region of interest (ROI). Contact ROIs that overlapped with the gray matter were selected and projected to the surface by sampling from five different positions between the white and pial surfaces (i.e., 0, 20, 40, 60, 80, and 100% of the distance between the two surfaces) using trilinear interpolation. The resulting five surface-projected ROIs for each contact were summed and binarized to produce a single cortical surface ROI for each electrode contact.

BOLD Functional Connectivity Analysis. Functional connectivity was estimated using surface-projected data using seed-based correlation procedures, similar to those previously described in refs. 47 and 48. Pair-wise Pearson's product–moment correlations between the fMRI timeseries at each vertex were computed, yielding an 81,924 × 81,924 correlation matrix (40,962 vertices per hemisphere) for each run of BOLD data. These matrices were Fisher transformed and averaged together, yielding a within-subject across-run mean correlation matrix. This average matrix was then inverse Fisher transformed back to correlation values and assigned to the vertices of a cortical surface template created in ref. 48. This template allowed individual vertices to be selected for real-time visualization of the resulting correlation maps using the Connectome Workbench's wb_view software. We probed the BOLD functional connectivity of the electrode sites of interest using two approaches.

Individual Network Mapping Using fMRI. As noted, resting-state fMRI data were collected from the patient some weeks prior to surgery in a single session. Three runs of data were collected leading to a total of 21 min of data for network estimation using intrinsic functional connectivity. fMRI data were processed using the iProc pipeline, which was built with the aim of optimizing interrun registration of functional images acquired from the same individual, while minimizing spatial blurring by performing registrations using a single interpolation. In previous work, the DMN was found to comprise two closely juxtaposed, parallel, and interdigitated networks when defined within the individual (47). The two systems were labeled default network A (DN-A) and B (DN-B) for convenience. Here, we sought to recapitulate those previous findings, as a means to best estimate the functional organization within DMN regions in the patient. In our previous work, although the two networks, DN-A and DN-B, displayed idiosyncrasies across individuals, consistent broad features were observed that helped build confidence that the same networks were being defined in different individuals. Primarily, both networks contained regions that were located within the bounds of the group-defined DMN throughout the brain. Next, consistent relationships were observed in the relative positions of the two networks' regions in key locations. Three major features of relevance to the present study are the following: 1) DN-A included a ventral PMC region that extended into retrosplenial cortex, while DN-B contained a more dorsal PMC region situated in posterior cingulate cortex, which was often surrounded on three sides by regions belonging to DN-A; 2) DN-A included a region in or near to the posterior angular gyrus, while a neighboring and more anterior parietal DN-B region was consistently observed closer to the TPJ; and 3) DN-A contained a region along the posterior parahippocampal cortex, while DN-B did not. These same features were used in the present analyses to help determine that DN-A and DN-B were being correctly defined.

BOLD images can be distorted due to magnetic field inhomogeneities that result from the BOLD contrast weighting. Hence, cross-modal registration from BOLD to T1 can be difficult to achieve accurately due to the two types of images having slightly different morphologies. Here, special attention was taken to ensure that the registration of BOLD and T1 data were accurate to help build confidence in the estimated location of the electrodes with regards to the network anatomy. It is important to note that perfect registration may be impossible to achieve and that, despite our best efforts, it is possible that some misalignment persists. For this reason, we display the registration in *SI Appendix*, Fig. S5 so that the reader can fully understand the degree of alignment between the different image types and interpret our results accordingly. The white matter boundary from the T1 (*SI Appendix*, Fig. S5, blue lines) closely encapsulated the white anatomy in the BOLD image, indicating good alignment.

Experimental iEEG Data Acquisition. iEEG data were recorded at the patient's bedside with a Nihon Kohden clinical monitoring system using a sampling rate of 1,000 Hz (bandpass filter: 1.6 to 300 Hz). Data were acquired during two conditions: 1) resting state (four recording runs, 20.3 min total), the patient visually fixated on a cross in the center of a laptop screen and was instructed to not think about anything in particular, and 2) cognitive task (three recording runs, 15.3 min total), the patient performed the gradual onset, continuous performance task, as described elsewhere (41). Data were rereferenced online to the most electrographically silent channel. Patient also performed episodic memory recall task, as described in our previous publications (57, 58, 61).

iEEG Functional Connectivity Analysis. iEEG functional connectivity analysis was performed, as described previously (42). A notch filter was applied to attenuate power-line noise (zero phase, third-order butterworth filter with band stop between 57 to 63, 117 to 123, and 177 to 183 Hz). Channel data were then rereferenced to the common average signal. We performed time–frequency decomposition on the continuous time series with a Morlet wavelet transform method for frequencies within the 70 to 170 Hz range (spaced by increments of 10), also known as the HFB range. We then normalized the distributions of power amplitude estimates by rescaling each time sample by the log ratio of each whole recording's time series (i.e., to account for 1/*f* decline of the power spectrum) and averaged those normalized estimates across all frequencies within the 70 to 170 Hz range. The HFB power amplitude was then filtered (zero phase, butterworth, and fourth order) between 0.1 to 1 Hz (42). Within each recording run, functional connectivity between channels was computed as the correlation coefficient between continuous, filtered HFB power amplitude estimates.

CCEP Data Acquisition and Analysis. Single-pulse stimulations were performed with a bipolar setup using a cortical stimulator. The patient was awake and resting. Single pulses of electrical current (3 mA, biphasic, and 400 μs/phase) were injected into pairs of intracranial electrodes at a frequency of 0.5 Hz for 100 pulses. Electrode voltages were recorded in all other nonstimulated electrodes with a sampling rate of 1,000 Hz. To minimize effects from volume conduction, data recorded from electrodes on the same shaft, as the stimulated electrodes, were discarded. Voltages were first rereferenced to a bipolar montage and evoked responses in nonstimulated electrodes were split into 325-ms trials around the stimulus, including 25 ms prestimulus signal and 300 ms poststimulus signal. All trials were averaged, and the resultant time series was normalized to the mean and SD of the prestimulus voltage. Peaks were automatically detected using MATLAB's peak detection algorithm, with a minimum peak prominence of five times the SD of the prestimulus signal. The time to the largest peak was taken as a metric for the connectivity between the stimulated electrodes and the recorded electrodes.

Data Availability. Anonymized fMRI and iEEG data have been deposited in Figshare (10.6084/m9.figshare.14675505; 10.6084/m9.figshare.14675415). All other study data are included in the article and/or supporting information.

ACKNOWLEDGMENTS. We thank Harinder Kaur, Thi Pham, and Luida Schumacher as clinical EEG technologists providing support during the research recordings; Gary Glover and Ross Mair for assistance with the setting up of the MRI scanning sequences; and Karl Deisseroth, Sam Vesuna, and Kieran Fox for helpful comments. We acknowledge a generous gift from the Bell Family to J.P., National Institute of Mental Health K99 Grant to R.M.B., Canadian Institutes of Health Research Banting Fellowship to A.K., and Stanford Medical Scholar Fellowship to M.J.V. The work was supported by Grant 1R21NS113024 to J.P.

1. M. E. Raichle *et al*., A default mode of brain function. *Proc. Natl. Acad. Sci. U.S.A.* **98**, 676–682 (2001).
2. P. Fransson, G. Marrelec, The precuneus/posterior cingulate cortex plays a pivotal role in the default mode network: Evidence from a partial correlation network analysis. *Neuroimage.* **42**, 1178–1184 (2008).
3. R. L. Buckner *et al*., Cortical hubs revealed by intrinsic functional connectivity: Mapping, assessment of stability, and relation to Alzheimer's disease. *J. Neurosci.* **29**, 1860–1873 (2009).
4. P. Hagmann *et al*., Mapping the structural core of human cerebral cortex. *PLoS Biol.* **6**, e159 (2008).
5. D. L. Schacter, D. R. Addis, R. L. Buckner, Remembering the past to imagine the future: The prospective brain. *Nat. Rev. Neurosci.* **8**, 657–661 (2007).
6. K. Christoff, Z. C. Irving, K. C. R. Fox, R. N. Spreng, J. R. Andrews-Hanna, Mind-wandering as spontaneous thought: A dynamic framework. *Nat. Rev. Neurosci.* **17**, 718–731 (2016).
7. N. C. Andreasen *et al*., Remembering the past: Two facets of episodic memory explored with positron emission tomography. *Am. J. Psychiatry* **152**, 1576–1585 (1995).
8. J. R. Binder *et al*., Conceptual processing during the conscious resting state. A functional MRI study. *J. Cogn. Neurosci.* **11**, 80–95 (1999).
9. E. Kross, *Chatter: The Voice in Our Head, Why It Matters, and How to Harness It* (Crown, 2021).
10. G. L. Shulman *et al*., Common blood flow changes across visual tasks: II. Decreases in cerebral cortex. *J. Cogn. Neurosci.* **9**, 648–663 (1997).
11. D. A. Gusnard, M. E. Raichle, M. E. Raichle, Searching for a baseline: Functional imaging and the resting human brain. *Nat. Rev. Neurosci.* **2**, 685–694 (2001).
12. P. Fiset *et al*., Brain mechanisms of propofol-induced loss of consciousness in humans: A positron emission tomographic study. *J. Neurosci.* **19**, 5506–5513 (1999).
13. S. Laureys, C. Lemaire, P. Maquet, C. Phillips, G. Franck, Cerebral metabolism during vegetative state and after recovery to consciousness. *J. Neurol. Neurosurg. Psychiatry* **67**, 121 (1999).
14. J. Parvizi, G. W. Van Hoesen, J. Buckwalter, A. Damasio, Neural connections of the posteromedial cortex in the macaque. *Proc. Natl. Acad. Sci. U.S.A.* **103**, 1563–1568 (2006).
15. J. P. Aggleton, R. Desimone, M. Mishkin, The origin, course, and termination of the hippocampothalamic projections in the macaque. *J. Comp. Neurol.* **243**, 409–421 (1986).
16. P. Fransson, Spontaneous low-frequency BOLD signal fluctuations: An fMRI investigation of the resting-state default mode of brain function hypothesis. *Hum. Brain Mapp.* **26**, 15–29 (2005).
17. I. N. Mavridis, T. Kalamatianos, C. Koutsarnakis, G. Stranjalis, Microsurgical anatomy of the precuneal artery: Does it really exist? Clarifying an ambiguous vessel under the microscope. *Oper. Neurosurg. (Hagerstown)* **12**, 68–76 (2016).
18. T. Kalamatianos *et al*., The parieto-occipital artery revisited: A microsurgical anatomic study. *World Neurosurg.* **126**, e1130–e1139 (2019).
19. J. Parvizi, S. Kastner, Promises and limitations of human intracranial electroencephalography. *Nat. Neurosci.* **21**, 474–483 (2018).
20. W. Penfield, E. Boldrey, Somatic motor and sensory representation in the cerebral cortex of man as studied by electrical stimulation. *Brain* **60**, 389–443 (1937).
21. B. L. Foster, J. Parvizi, Direct cortical stimulation of human posteromedial cortex. *Neurology* **88**, 685–691 (2017).
22. F. Caruana *et al*., Motor and emotional behaviours elicited by electrical stimulation of the human cingulate cortex. *Brain* **141**, 3035–3051 (2018).
23. K. C. R. Fox *et al*., Intrinsic network architecture predicts the effects elicited by intracranial electrical stimulation of the human brain. *Nat. Hum. Behav.* **4**, 1039–1052 (2020).
24. V. S. Natu *et al*., Stimulation of the posterior cingulate cortex impairs episodic memory encoding. *J. Neurosci.* **39**, 7173–7182 (2019).
25. M.-L. Read, R. Lissaman, Commentary: Stimulation of the posterior cingulate cortex impairs episodic memory encoding. *Front. Hum. Neurosci.* **14**, 334 (2020).
26. A. Vogrig *et al*., A systematic study of stereotypy in epileptic seizures versus psychogenic seizure-like events. *Epilepsy Behav.* **90**, 172–177 (2019).
27. J. Bancaud, J. Talairach, Clinical semiology of frontal lobe seizures. *Adv. Neurol.* **57**, 3–58 (1992).
28. S. Umeoka *et al*., Bilateral symmetric tonic posturing suggesting propagation to the supplementary motor area in a patient with precuneate cortical dysplasia. *Epileptic Disord.* **9**, 443–448 (2007).
29. M. Z. Koubeissi, C. C. Jouny, J. O. Blakeley, G. K. Bergey, Analysis of dynamics and propagation of parietal cingulate seizures with secondary mesial temporal involvement. *Epilepsy Behav.* **14**, 108–112 (2009).
30. R. Alkawadri, N. K. So, P. C. Van Ness, A. V. Alexopoulos, Cingulate epilepsy: Report of 3 electroclinical subtypes with surgical outcomes. *JAMA Neurol.* **70**, 995–1002 (2013).
31. R. Enatsu *et al*., Posterior cingulate epilepsy: Clinical and neurophysiological analysis. *J. Neurol. Neurosurg. Psychiatry* **85**, 44–50 (2014).
32. J. Mailo, R. Tang-Wai, Insight into the precuneus: A novel seizure semiology in a child with epilepsy arising from the right posterior precuneus. *Epileptic Disord.* **17**, 321–327 (2015).
33. I. Doležalová, M. Brázdil, P. Kahane, Temporal lobe epilepsy? Things are not always what they seem. *Epileptic Disord.* **19**, 59–66 (2017).
34. Y. Yang *et al*., Electroclinical characteristics of seizures arising from the precuneus based on stereoelectroencephalography (SEEG). *BMC Neurol.* **18**, 110 (2018).
35. S. Pendekanti, S. Baek, Y. B. Kilinc, J. Parvizi, High-level visual manifestations of epileptic seizures originating from the medial parietal cortex. *Epileptic Disord.* **20**, 200–203 (2018).
36. C.-C. Chou *et al*., Cingulate gyrus epilepsy: Semiology, invasive EEG, and surgical approaches. *Neurosurg. Focus* **48**, E8 (2020).
37. A. Harroud *et al*., Precuneal epilepsy: Clinical features and surgical outcome. *Epilepsy Behav.* **73**, 77–82 (2017).
38. S. Vesuna *et al*., Deep posteromedial cortical rhythm in dissociation. *Nature* **586**, 87–94 (2020).
39. G. Spena *et al*., Preoperative and intraoperative brain mapping for the resection of eloquent-area tumors. A prospective analysis of methodology, correlation, and usefulness based on clinical outcomes. *Acta Neurochir. (Wien)* **152**, 1835–1846 (2010).
40. Y. Nir *et al*., Coupling between neuronal firing rate, gamma LFP, and BOLD fMRI is related to interneuronal correlations. *Curr. Biol.* **17**, 1275–1285 (2007).
41. A. Kucyi *et al*., Electrophysiological dynamics of antagonistic brain networks reflect attentional fluctuations. *Nat. Commun.* **11**, 325 (2020).
42. A. Kucyi *et al*., Intracranial electrophysiology reveals reproducible intrinsic functional connectivity within human brain networks. *J. Neurosci.* **38**, 4230–4242 (2018).
43. B. L. Foster, V. Rangarajan, W. R. Shirer, J. Parvizi, Intrinsic and task-dependent coupling of neuronal population activity in human parietal cortex. *Neuron* **86**, 578–590 (2015).
44. R. Matsumoto *et al*., Functional connectivity in the human language system: A cortico-cortical evoked potential study. *Brain* **127**, 2316–2330 (2004).
45. J. M. Shine *et al*., Distinct patterns of temporal and directional connectivity among intrinsic networks in the human brain. *J. Neurosci.* **37**, 9667–9674 (2017).
46. B. T. T. Yeo *et al*., The organization of the human cerebral cortex estimated by intrinsic functional connectivity. *J. Neurophysiol.* **106**, 1125–1165 (2011).
47. R. M. Braga, K. R. A. Van Dijk, J. R. Polimeni, M. C. Eldaief, R. L. Buckner, Parallel distributed networks resolved at high resolution reveal close juxtaposition of distinct regions. *J. Neurophysiol.* **121**, 1513–1534 (2019).
48. R. M. Braga, R. L. Buckner, Parallel interdigitated distributed networks within the individual estimated by intrinsic functional connectivity. *Neuron* **95**, 457–471.e5 (2017).
49. T. O. Laumann *et al*., Functional system and areal organization of a highly sampled individual human brain. *Neuron* **87**, 657–670 (2015).
50. L. M. DiNicola, R. M. Braga, R. L. Buckner, Parallel distributed networks dissociate episodic and social functions within the individual. *J. Neurophysiol.* **123**, 1144–1179 (2020). Correction in: *J. Neurophysiol.* **124**, 307 (2020).
51. R. M. Braga, L. M. DiNicola, H. C. Becker, R. L. Buckner, Situating the left-lateralized language network in the broader organization of multiple specialized large-scale distributed networks. *J. Neurophysiol.* **124**, 1415–1448 (2020).
52. B. Fischl, FreeSurfer. *Neuroimage* **62**, 774–781 (2012).
53. American Psychiatric Association, *Diagnostic and Statistical Manual of Mental Disorders: Fifth Edition (DSM-5)* (American Psychiatric Publishing, ed. 5, 2013).
54. O. Blanke, S. Ortigue, T. Landis, M. Seeck, Stimulating illusory own-body perceptions. *Nature* **419**, 269–270 (2002).
55. S. Ionta *et al*., Multisensory mechanisms in temporo-parietal cortex support self-location and first-person perspective. *Neuron* **70**, 363–374 (2011).
56. K. C. R. Fox, B. L. Foster, A. Kucyi, A. L. Daitch, J. Parvizi, Intracranial electrophysiology of the human default network. *Trends Cogn. Sci.* **22**, 307–324 (2018).
57. A. L. Daitch, J. Parvizi, Spatial and temporal heterogeneity of neural responses in human posteromedial cortex. *Proc. Natl. Acad. Sci. U.S.A.* **115**, 4785–4790 (2018).
58. M. Dastjerdi *et al*., Differential electrophysiological response during rest, self-referential, and non-self-referential tasks in human posteromedial cortex. *Proc. Natl. Acad. Sci. U.S.A.* **108**, 3023–3028 (2011).
59. T. Ossandón *et al*., Transient suppression of broadband gamma power in the default-mode network is correlated with task complexity and subject performance. *J. Neurosci.* **31**, 14521–14530 (2011).
60. S. Liu, J. Parvizi, Cognitive refractory state caused by spontaneous epileptic high-frequency oscillations in the human brain. *Sci. Transl. Med.* **11**, eaax7830 (2019).
61. B. L. Foster, M. Dastjerdi, J. Parvizi, Neural populations in human posteromedial cortex display opposing responses during memory and numerical processing. *Proc. Natl. Acad. Sci. U.S.A.* **109**, 15514–15519 (2012).